Transp Porous Med (2011) 89:213–236
DOI 10.1007/s11242-011-9765-2

Fractional Flow Theory Applicable to Non-Newtonian Behavior in EOR Processes

W. R. Rossen · A. Venkatraman · R. T. Johns · K. R. Kibodeaux · H. Lai · N. Moradi Tehrani

Received: 9 November 2010 / Accepted: 6 April 2011 / Published online: 21 April 2011

Abstract The method of characteristics, or fractional-flow theory, is extremely useful in understanding complex Enhanced Oil Recovery (EOR) processes and in calibrating simulators. One limitation has been its restriction to Newtonian rheology except in rectilinear flow. Its inability to deal with non-Newtonian rheology in polymer and foam EOR has been a serious limitation. We extend fractional flow methods for two-phase flow to non-Newtonian fluids in one-dimensional cylindrical flow, where rheology changes with distance from injection well. The fractional flow curve is then a function of position and we analyze the characteristic equations for two applications—polymer and foam floods. For polymer flooding, we present a semi-analytical solution for the changing fractional flow curve where characteristics and shocks collide. The semi-analytical solution is shown to give good agreement with the finite-difference simulation thus helping us understand the development and resolution of shocks. We discuss two separate cases of foam injection with or without preflush. We observe that the fractional flow solutions are more accurate than finite-difference simulations on a comparable grid and hence the method can be used to calibrate simulators. For SAG (alternating-slug) foam injection, characteristics and shocks collide, making the fractional-flow solution complex. Nonetheless, one can solve exactly for changing mobility near the well, to greater accuracy than with conventional simulation. The fractional-flow method extended to non-Newtonian flow can be useful both for its insights for scale-up of laboratory experiments and to calibrate computer simulators involving non-Newtonian EOR. It can also be an input to streamline simulations.

W. R. Rossen, N. M. Tehrani
Delft University of Technology, Delft, The Netherlands

A. Venkatraman (✉) · H. Lai
The University of Texas at Austin, Austin, TX, USA
e-mail: ashwin.venkatraman@mail.utexas.edu

R. T. Johns
Penn State University, University Park, PA, USA

K. R. Kibodeaux
Shell Exploration and Production Co, Houston, TX, USA

Keywords Fractional flow · Non-Newtonian fluid · Polymer · Foam · Shocks

1 Introduction

Fractional flow methods or more formally the method of characteristics (MOC) have proved essential in simplifying and understanding oil-recovery processes, especially enhanced oil recovery (EOR) processes (Pope 1980; Lake 1989; Walsh and Lake 1989). In many cases, EOR processes involving multiple components can be represented by two-phase fractional flow solutions, often involving a jump in the concentration of some chemical component within one phase. Despite simplifying assumptions, the MOC predicts the solution structure of displacements well, even when those assumptions are relaxed. Solutions using the MOC, however, typically assume Newtonian viscosities of all phases.

Many EOR processes, especially polymer and foam EOR, involve non-Newtonian phase viscosities. MOC solutions for displacements in these EOR processes provide important insights, but have not described the effect of non-Newtonian viscosities on the displacements.

In radial or streamline flow, non-Newtonian phase viscosities imply that the fractional flow function varies with position along the streamline. In rectilinear 1D flow, there is a single fractional flow function that applies to the entire displacement even for non-Newtonian fluids; see Wu et al. (1991, 1992) and Yi (2004). Wu et al. (1995) and Subramanian et al. (1997, 1999) give solutions for dynamic 1D displacements where flow is from one porous medium to another with a different fractional flow function. Bedrikovetsky (1993) briefly gives the solution for one-dimensional (1D) gravity drainage in a dome-shaped reservoir with an expanding gas cap. The relative contributions of gravity and viscous effects change with the cross-sectional area of the dome, which depends on vertical coordinate z; therefore a different fractional flow function applies at each value of z. Jamshidnezhad et al. (2008) present a solution for steady-state gravity segregation in 2D cylindrical flow for non-Newtonian fluids using the MOC.

In this article, we describe a framework for modeling 1D dynamic displacement with non-Newtonian phase viscosities using the MOC, with numerical simulations provided for comparison. We illustrate the method with several cases where the fractional flow curve changes with radial distance. For injection of non-Newtonian foam following a surfactant preflush, a simple, exact solution is possible. Without the preflush, a solution is possible that is exact for the foam bank and approximately correct for the gas bank that precedes the foam bank. For injection of non-Newtonian polymer or injection of foam in alternating slugs of gas and liquid (SAG injection), an exact solution using MOC is also possible, though more complex. It is relatively simple, however, to solve exactly for mobility behind the chemical shock, i.e., in the near-wellbore region crucial to injectivity. Analysis of the problem in terms of the changing fractional flow curve provides insights into how the process proceeds.

2 Theory

Except for allowing non-Newtonian phase viscosities, we make the usual assumptions of fractional flow theory (Pope 1980; Lake 1989):

1. The 1D cylindrical reservoir is homogeneous, with uniform thickness, with inner radius r_w and an open outer boundary at r_e. We also assume $r_e >> r_w$.

2. Only two mobile phases are present, though a third immobile phase (e.g., residual oil in a foam flood) may be present.
3. Fluids are injected at the inner boundary $r = r_w$ at fixed total volumetric rate Q and fractional flow of water $f_w = f_w^J$.
4. Phases are incompressible, and components are each soluble only in one phase. In principle, adsorption of chemicals from the aqueous phase onto rock surface is allowed, though for simplicity we neglect it in the examples shown below.
5. Dispersive processes, including fingering, capillary diffusion, and dispersion, are negligible.
6. There is instantaneous attainment of local steady-state mobilities, which depend only on local saturations.
7. There are no chemical or biological reactions.

We define dimensionless variables x_D and t_D as usual for cylindrical flow:

$$x_D = \frac{r^2 - r_w^2}{r_e^2 - r_w^2} \cong \frac{r^2}{r_e^2} \qquad t_D = \frac{Qt}{\pi \left(r_e^2 - r_w^2\right) H_e \phi} \cong \frac{Qt}{\pi r_e^2 H_e \phi} \tag{1}$$

where H_e is the height and ϕ the porosity of the reservoir. The governing differential equation is

$$\frac{\partial S_w}{\partial t_D} + \frac{\partial f_w}{\partial x_D} = 0 \tag{2}$$

We consider the case where f_w depends on both S_w and x_D:

$$\frac{\partial f_w}{\partial x_D} = \left(\frac{\partial f_w}{\partial S_w}\right)_{x_D} \frac{\partial S_w}{\partial x_D} + \left(\frac{\partial f_w}{\partial x_D}\right)_{S_w} \tag{3}$$

Inserting Eq. 3 into Eq. 2 leads to:

$$\frac{\partial S_w}{\partial t_D} + \left(\frac{\partial f_w}{\partial S_w}\right)_{x_D} \frac{\partial S_w}{\partial x_D} = -\left(\frac{\partial f_w}{\partial x_D}\right)_{S_w} \tag{4}$$

Equation 4 can be classified as a non-homogeneous quasi-linear partial differential equation with characteristic equations given by (η varies along a characteristics),

$$\frac{dS_w}{d\eta} = -\left(\frac{\partial f_w}{\partial x_D}\right)_{S_w} \tag{5}$$

$$\frac{dx_D}{d\eta} = \left(\frac{\partial f_w}{\partial S_w}\right)_{x_D} \tag{6}$$

$$\frac{dt_D}{d\eta} = 1 \tag{7}$$

Characteristics move with a velocity given by:

$$\frac{dx_D}{dt_D} = \left(\frac{\partial f_w}{\partial S_w}\right)_{x_D} \tag{8}$$

The characteristics are not straight lines because the velocity of a characteristic can change as x_D changes (Eq. 8). Shocks can also form, in which its velocity can also vary radially. The non-homogeneous aspect of Eq. 4 implies that S_w is not constant along a characteristic

and varies according to Eq. 5. We can also show that f_w is constant along the characteristics (Bedrikovetsky 1993) by applying Eqs. 2 and 8:

$$\left(\frac{\partial S_w}{\partial t_D}\right)_{x_D} + \left(\frac{\partial f_w}{\partial x_D}\right)_{t_D} = \left(\frac{\partial S_w}{\partial t_D}\right)_{x_D} \left(\frac{\partial f_w}{\partial S_w}\right)_{x_D} \left(\frac{dx_D}{dt_D}\right)^{-1}_{\text{char}} + \left(\frac{\partial f_w}{\partial x_D}\right)_{t_D} = 0 \quad (9)$$

$$\left(\frac{\partial f_w}{\partial t_D}\right)_{x_D} \left(\frac{dx_D}{dt_D}\right)^{-1}_{\text{char}} + \left(\frac{\partial f_w}{\partial x_D}\right)_{t_D} = \left(\frac{\partial f_w}{\partial x_D}\right)_{\text{char}} = 0 \quad (10)$$

We analyze the equations developed in this section for two applications: polymer and foam floods. We obtain solutions to the differential equations by extending the fractional flow theory.

3 Application to Polymer Injection

In this section, we develop the characteristic equations for non-Newtonian polymer floods and give an example solution for a particular set of input parameters. We highlight the implications of the solution structure in the context of fractional flow theory that is used to solve this particular case of polymer injection.

3.1 Model Description

The non-Newtonian behavior is introduced by modeling polymer water solution as a power-law fluid. Many polymer solutions obey shear-thinning power-law rheology over some range of shear rates, with Newtonian behavior at lower shear rate and complex behavior at higher shear rates (Lake 1989). The exact correspondence between shear rate in a viscometer and interstitial velocity in a porous medium is complex. AlSofi and Blunt (2010) have recently developed a non-Newtonian polymer flooding model for streamline simulation where they combine the viscosifying and the non-Newtonian effects using a multiplier approach (similar to commercial simulators).

We introduce non-Newtonian rheology by modeling the polymer water as a power- law fluid and shear-thinning rheology (Venkatraman et al. 2011). This results in an implicit formulation for f_w (Appendix A) that is given by,

$$f_w = \frac{1}{1 + \frac{k_o \mu_w^o}{k_w \mu_o} \left(\frac{Q_D f_w}{\sqrt{x_D} S_w}\right)^{n-1}}. \quad (11)$$

Here k_o and k_w are the relative permeability functions for oleic and aqueous phases, respectively, and μ_o is the viscosity of the oleic phase. We assume a Corey type relative permeability relation and summarize the characteristic equations in terms of function $H(x_D, S_w)$ (from Eq. A9 described in Appendix A).

$$\frac{dS_w}{d\eta} = -\left(\frac{\partial f_w}{\partial x_D}\right)_{s_w} = \frac{-f_w^n \left(\frac{\partial H}{\partial x_D}\right)_{s_w}}{1 + nHf_w^{n-1}} \quad (12)$$

$$\frac{dx_D}{d\eta} = \left(\frac{\partial f_w}{\partial S_w}\right)_{x_D} = \frac{-f_w^n \left(\frac{\partial H}{\partial S_w}\right)_{x_D}}{1 + nHf_w^{n-1}} \quad (13)$$

$$\frac{\mathrm{d}t_{\mathrm{D}}}{\mathrm{d}\eta} = 1 \tag{14}$$

One approach to obtain the general solution for the quasi-linear partial differential equation is by combining any two characteristic equations (from Eqs. 12–14) and solving analytically to get two surfaces (Rhee et al. 1986). The intersection of these two surfaces is then the desired solution.

In our attempt to solve these equations analytically, we observe that combining Eqs. 12 and 13 results in function H being a constant along the characteristics (see Appendix A). This implies f_{w} is a constant (Eq. A10) along the characteristic, a fact that we proved earlier (Eq. 10). It is, however, difficult to analytically solve the other two combinations from equations Eqs. 12–14 considering that H is a complicated function of x_{D} and S^{w}.

We choose to relate the above problem using fractional flow theory, widely used to formulate polymer flooding. The MOC solution for injection of a polymer modeled as a Newtonian fluid is a single Riemann problem described by Lake (1989). There are two fractional flow curves: one with polymer and one without. In this discussion, we refer to the curve with polymer as the polymer–oil fractional flow curve and the one without polymer is the oil–water fractional flow curve. In the conventional theory, the oil–water curve is fixed and the polymer is assumed to have a constant viscosity that results in fixed polymer–oil curve. However, in the case of non-Newtonian polymer, the polymer–oil curve is dependent on distance from injection well x_{D} (Eq. 11) and hence changes continuously.

We resolve the changing fractional flow by dividing the entire displacement into many small intervals, where the fractional flow curve is fixed for each interval. This results in a semi-analytical solution. In the next section, we explain the construction of a semi-analytical solution by illustrating it for a specific non-Newtonian behavior (case of $n = 0.5$ in Eq. 11). We shall compare the semi-analytical solution with that obtained using finite difference simulation and explain the development of shocks and their resolution as they collide.

3.2 Semi-Analytical Solution Construction

We consider three species (polymer, water and oil) and two phases (aqueous and oleic) and construct the solution for a 1D radial displacement problem. We take initial condition I as $S_{wI} = 0.3$ on the oil–water fractional flow curve and the residual water saturation as well as the residual oil saturation is 0.3. In this particular example, the injection condition J is at $f_{\mathrm{w}} = 1$ on the polymer–oil fractional flow curve. We also assume that the viscosity of polymer solution is constant for large and small water interstitial velocities, at 0.003 and 0.03 Pa s, respectively. In between, polymer–solution viscosity scales with interstitial velocity of water according to a power-law relation,

$$\mu_{\mathrm{w}} = \mu_{\mathrm{w}}^{\mathrm{o}} \left(\frac{u f_{\mathrm{w}}}{v_{\mathrm{w}}^{\mathrm{o}} S_{\mathrm{w}} \phi} \right)^{-0.5}. \tag{15}$$

In Eq.15, we have selected the power-law exponent $n = 0.5$ and develop expressions for f_{w} for this particular case (see Appendix A). The position-dependent velocity of the characteristics is then given by:

$$\left(\frac{\partial f_{\mathrm{w}}}{\partial S_{\mathrm{w}}} \right)_{x_{\mathrm{D}}} = H \left(H - \frac{H^2 + 2}{\sqrt{H^2 + 4}} \right) \left(\frac{-n_0}{(1 - S)(1 - S_{\mathrm{rw}} - S_{\mathrm{ro}})} + \frac{(-n_{\mathrm{w}})}{S(1 - S_{\mathrm{rw}} - S_{\mathrm{ro}})} + \frac{(1 - n)}{S_{\mathrm{w}}} \right) \tag{16}$$

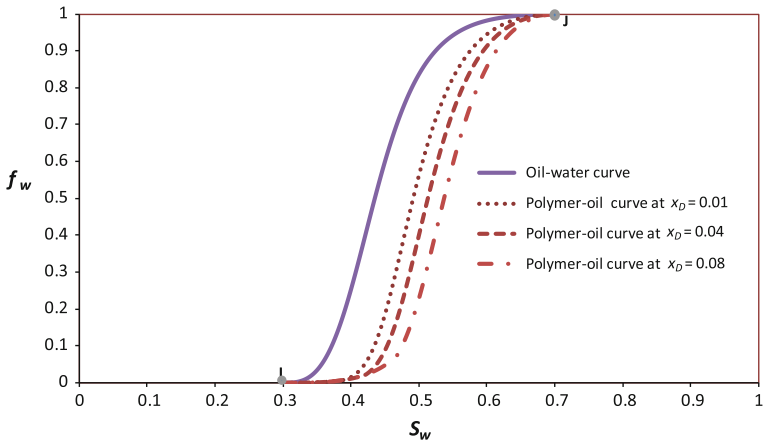

Fig. 1 The oil–water and polymer–oil fractional flow curves using parameter values from Table 1. The polymer–oil curve changes with increasing distance ($x_{\mathrm{D}} = 0.01, 0.04,$ and 0.04) from the injection well, while the oil–water curve is fixed

As the distance from the injection well increases, the superficial velocity decreases and the viscosity of the polymer increases. Thus the polymer–oil fractional flow curve changes continuously with increasing distance (Fig. 1). We construct an equivalent problem where we divide the distances into various intervals Δx_{D} such that the fractional flow curve is constant in every interval and is assumed to change only at the interface. In the limit of this interval approaching zero, the two problems are equivalent. At the points of discontinuity where the fractional flow curve changes, the saturations are translated onto the new curves such that f_{w} is constant (and hence H is also constant).

The chemical shock and the Buckley–Leverett (BL) shock change at the interfaces and can be analyzed by considering it to be series of Riemann problems with varying initial condition for each distance interval. Let us consider the first interval where we have both the oil–water and polymer–oil fractional flow curves. The solution construction in this interval is discussed by Lake (1989) where the solution is constructed from point I to point J. The BL shock velocity between the upstream and the downstream point is obtained from the oil–water fractional flow curve and a material balance on water. In Fig. 2, the upstream point is the point I (initial condition) and the downstream point is B_1 so that we have,

$$v_{\mathrm{BLshock}} = \frac{\Delta x_{\mathrm{D}}}{\Delta t_{\mathrm{D}}} = \frac{\left(f_{\mathrm{w}}^{\mathrm{D}} - f_{\mathrm{w}}^{U}\right)}{\left(S_{\mathrm{w}}^{\mathrm{D}} - S_{\mathrm{w}}^{\mathrm{D}}\right)} = \frac{\left(f_{\mathrm{w}}^{B_1} - f_{\mathrm{w}}^{I}\right)}{\left(S_{\mathrm{w}}^{B_1} - S_{\mathrm{w}}^{I}\right)} \tag{17}$$

Equation 17 represents the slope of the chord joining points B_1 and I. The change from the oil–water curve (point B_1) to the polymer–oil curve (point T_1) is given by a polymer material balance. Although it could be accounted for, we assume no adsorption of the polymer on the rock surface and no excluded or inaccessible pore volume. Also, the polymer concentration of point B_1 is zero. Thus the material balance on polymer can be simplified to get the chemical shock velocity as follows:

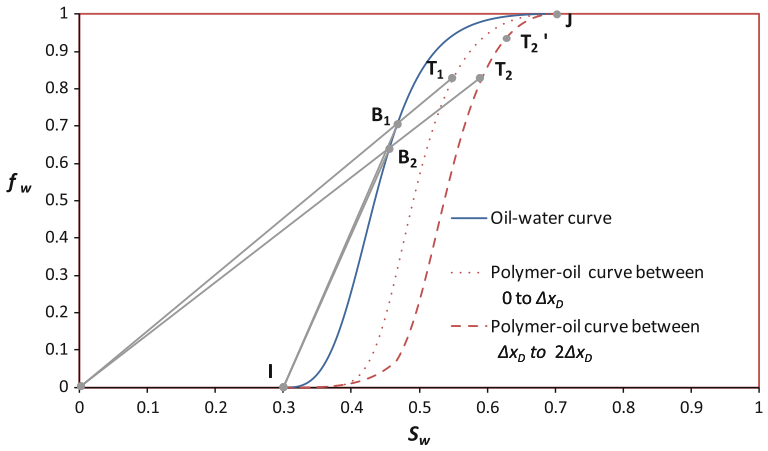

Fig. 2 The construction of solution for oil–water fractional flow curve and two polymer–oil fractional flow curves between consecutive intervals (0 to Δx_D) and (Δx_D to 2 Δx_D). The polymer–oil curves are constant within each interval

$$\left(Av f_w^{T_1} c_{pw}^{T_1} - Av f_w^{B_1} \underbrace{c_{pw}^{B_1}}_{0} \right) \Delta t = \left(A\phi S_w^{T_1} c_{pw}^{T_1} - A\phi S_w^{B_1} \underbrace{c_{pw}^{B_1}}_{0} + \underbrace{A(1-\phi)\delta_s}_{=0(\text{no adsorption})} \right) \Delta x \tag{18}$$

$$v_{\text{Chemical shock}} = \frac{f_w^{T_1}}{S_w^{T_1}} \tag{19}$$

Equation 19 represents the slope of a line drawn from the origin to the point T_1 on the polymer–oil fractional flow curve (see Fig 2).

According to the coherence condition, water and polymer at the same location move with the same velocity. Graphically, this implies that the chemical shock is the slope of the tangent line drawn from the origin to the polymer–oil fractional flow curve (point T_1) and this intersects the oil–water fractional flow curve at point B_1 (Fig. 2). The slope of the chord connecting points I and B_1 is the BL shock velocity. Thus, the solution for this interval has (1) a BL shock from I to B_1 with velocity given by Eq. 17, (2) a chemical shock from B_1 to T_1 with velocity given by Eq. 19, and (3) a rarefaction wave from point T_1 to J given by the derivative on a $f_w - S_w$ curve at point T_1 given by Eq. 16.

Point T_1 is translated to point T_2 for the next interval (Fig. 2) where the polymer–oil curve changes such that

$$(f_w)_{T_1} = (f_w)_{T_2} \tag{20}$$

This is a new Riemann problem for this interval where the solution is constructed from point B_1 to point J. Let B_2 be the point on the oil–water curve that connects to point T_2 on the polymer–oil curve. For this second interval, the chemical shock velocity is obtained by the polymer balance similar to Eq. 18,

Table 1 Parameters used for polymer example

Number of grid blocks N	5000/1000 (linear in $x_D \sim \sqrt{r}$)
Aqueous-phase viscosity	Max.: 0.03 Pa s, Min.: 0.003 Pa s, intermediate scaling according to Eq. 15
Q_D	5
Oil viscosity	0.02 Pa s
Water relative permeability function	$0.20\,[(S_w - 0.3)/0.4]^{2.82}$
Oil relative permeability function	$0.40\,[(0.7 - S_w)/0.4]^{1.87}$

$$\left(Avf_w^{T_2} c_{pw}^{T_2} - Avf_w^{B_2} \underbrace{c_{pw}^{B_2}}_{0} \right) \Delta t = \left(A\phi S_w^{T_2} c_{pw}^{T_2} - A\phi S_w^{B_2} \underbrace{c_{pw}^{B_2}}_{0} + \underbrace{A(1-\phi)\delta_s}_{=0(\text{no adsorption})} \right) \Delta x \tag{21}$$

$$v_{\text{Chemical shock}} = \frac{f_w^{T_2}}{S_w^{T_2}} \tag{22}$$

The chord connecting the origin and point T_2 intersects the oil–water fractional flow curve at point B_2. The solution for the new Riemann problem in this interval now consists of (1) an intermediate wave from point B_1 to B_2; (2) a chemical shock from point B_2 to T_2; and (3) a rarefaction wave from point T_2 to J.

The saturation velocities increase from B_1 to B_2 (for this particular case with model parameters as listed in Table 1), which results in the intermediate wave being a shock (henceforth referred to as an intermediate shock). The intermediate shock from B_1 to B_2 has the fastest velocity and impinges on the BL shock generated in the previous interval. These two shocks collide and hence the BL shock velocity changes to a new value indicated by the slope of the chord connecting points I and B_2 (Fig. 2).

Consider the chemical shock and the rarefaction wave from point T_2 to J following the chemical shock. It can be seen that some of the characteristics corresponding to the saturation velocities (immediately following point T_2) in the rarefaction-wave region of the solution intersect the chemical shock (see Fig. 3). This is because the saturation velocity at point T_2 (given by the derivative at point T_2) is greater than the polymer shock velocity (slope of chord B_2T_2). We resolve this by defining point T_2' in this fractional flow curve as the point beyond which the saturation velocities is less than the polymer shock velocity B_2T_2. This implies that the resolved polymer shock velocity for that interval is then B_2T_2'. The rarefaction waves and shocks corresponding to the above two intervals are represented in the $x_D - t_D$ diagram in Fig. 3.

Proceeding similarly, we can find for the last interval k, a point B_k on the oil–water fractional flow curve and a point T_k (refer Fig. 4) corresponding to the polymer fractional flow curves for the next intervals and a general solution can be constructed. It is reasonable to assume for simplicity that the section B_1B_k on the oil–water fractional flow curve is a straight line. Thus the intermediate fast shocks arising from points $B_1, B_2, \ldots, B_k$ that impinge on the BL shock have the same velocity as that of the chord connecting points B_1 and B_k. A schematic of the characteristics and shocks emanating for this displacement over the entire displacement are shown on the $x_D - t_D$ diagram in Fig. 5. It can be seen that the velocity

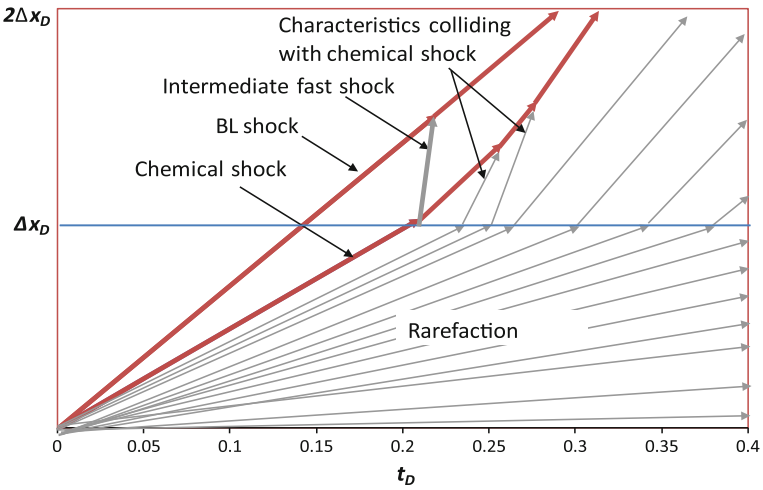

Fig. 3 Shock waves formed corresponding to polymer–oil curves that change in two consecutive intervals

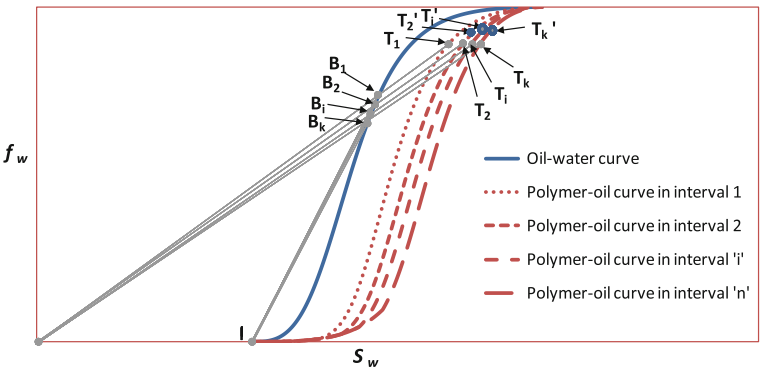

Fig. 4 The solution construction for several distance intervals

of the chemical shock increases, while the velocity of BL shock decreases with increasing distance from the injection well.

3.3 Finite-Difference Simulation

We have assumed $n = 0.5$ and that polymer solution viscosity is bounded by a maximum value of 0.03 Pa s and a minimum value of 0.003 Pa s for the simulation. We use a simple 1D incompressible, forward-difference, finite difference simulator to solve for water saturation and polymer concentration as a function of position and time (much as described in Appendix B for foam). For each time step, we solve

$$S_{wg}^{l+1} = S_{wg}^{l} + \frac{\Delta t_{\mathrm{D}}}{\Delta x_{\mathrm{D}}} \left(f_{wg-1}^{l} - f_{wg}^{l} \right) \tag{23}$$

for grid blocks $g = 1, \ldots, N_g$, where f_{w} is a function of both S_{wg} (water saturation at gird block g) and g. We used 1,000 and 5,000 grid blocks in the simulations to minimize

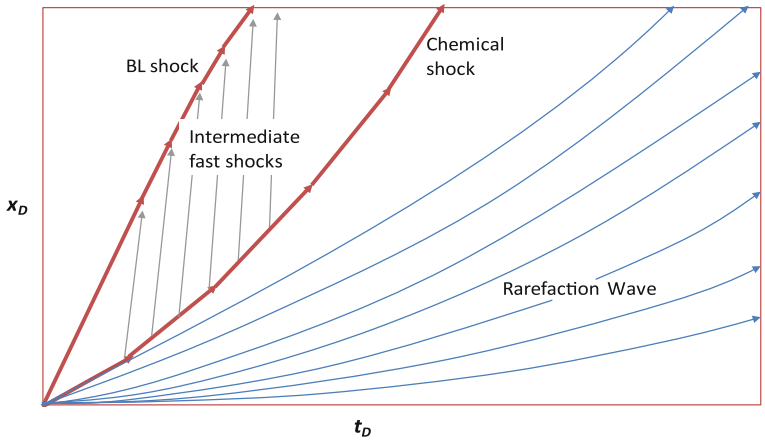

Fig. 5 A schematic of shocks formed over the entire interval showing collision and subsequent resolution

numerical dispersion. Because Eq. A4 is in dimensionless form, it is not necessary to specify dimensional quantities like permeability, porosity, injection rate, etc. The results are therefore presented in terms of these dimensionless parameters. The parameter values used for the finite difference method and the semi-analytical solution are listed in Table 1.

3.4 Results

The expressions for shock velocities (chemical and BL shock) along with the saturation velocities in the rarefaction wave developed in the previous section can be used to obtain semi-analytical solutions of saturation profiles. We divide the saturation profile into two regions: the rarefaction wave region and the shock region. The shock locations are calculated semi-analytically by assuming the velocity of these shocks to be a constant over a small interval as discussed in the previous section. Also, we have derived an expression for saturation velocity at a particular position (Eq. A12), which can be then used for the rarefaction region of the saturation profile.

The saturation profile for parameters as listed in Table 1 and for $t_{\mathrm{D}} = 0.2$ is shown in Fig. 6. The analytical solution is compared with the finite-difference scheme and we observe a good match for the small interval width ($\Delta x_{\mathrm{D}} = 0.0025$). As the interval width Δx_{D} is further decreased to 0.001, the maximum chemical-shock velocity increases so that an even better match is observed at the chemical shock location. This also results in more characteristics impinging the BL shock and hence reducing its velocity. The rarefaction-wave region of the saturation profile shows an excellent match between the semi-analytical solution and finite-difference simulations. Figures 7 and 8 are enlarged versions of Fig. 6 at shock regions of the saturation profile.

4 Application to Foam Displacements

We now focus on foam displacements where the solution includes a possible surfactant preflush. The cases discussed below highlight that one can map out the entire displacement to

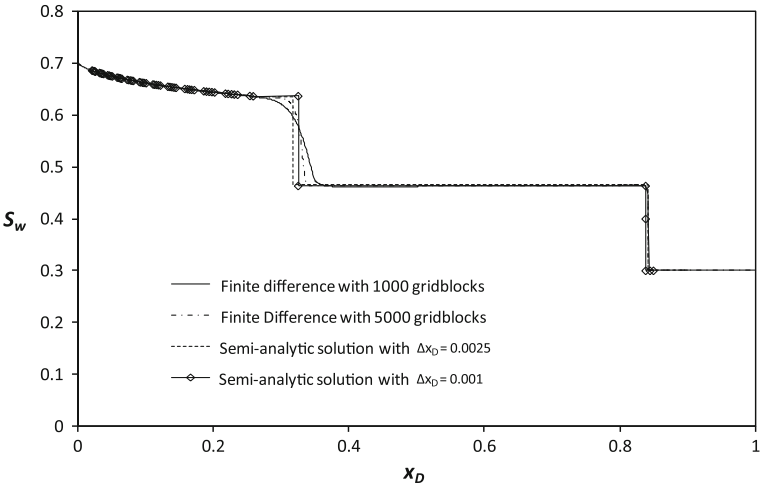

Fig. 6 A comparison of saturation profiles at $t_D = 0.2$ obtained using the finite difference method and the semi-analytical solution method with two distance interval lengths

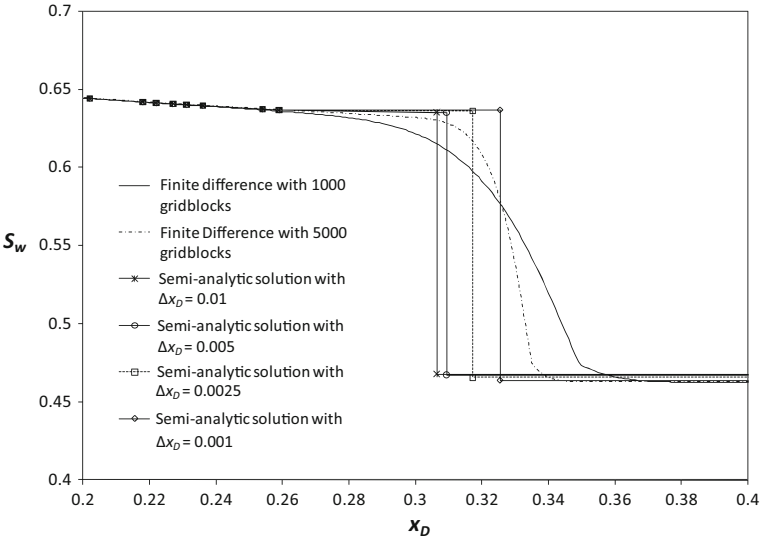

Fig. 7 Enlarged view of the comparison of the chemical shock location in the saturation profiles ($t_D = 0.2$) of Fig. 6. The match improves as interval length decreases and is best for $\Delta x_D = 0.001$

great accuracy with methods not much more complicated that MOC applied to Newtonian displacements.

4.1 Model

At steady state, "strong" (low-mobility) foams can be non-Newtonian, usually shear-thinning (Kovscek and Radke 1994; Rossen 1996; Alvarez et al. 2001; Rong 2002). Data on steady state foam mobility are available only over a relatively narrow range of injection rates

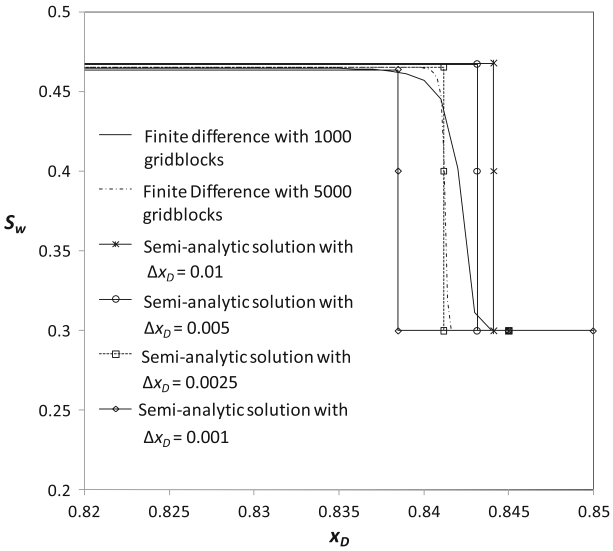

Fig. 8 Enlarged view of the comparison of the BL shock location for the saturation profiles ($t_{\mathrm{D}} = 0.2$) of Fig. 6. As interval lengths (Δx_{D}) are decreased, the location of BL shock moves toward the numerical solution, but under predicts its location as the distance interval decreases further. This is likely the result of more intermediate shocks impinging on the BL shock. The best match is observed for $\Delta x_{\mathrm{D}} = 0.0025$

compared to the variation of superficial velocity between a wellbore and the bulk of the formation. For illustration, we assume that the rheology of gas in foam is shear-thinning like a power-law fluid with a power-law exponent $n = 0.5$ (Bird et al. 2002), as described in Appendix B. If foam were Newtonian over some range of injection rates, one would determine which range of dimensionless position x_{D} this applies to and then map out the displacement in this range of x_{D} as a Newtonian displacement. The fractional flow curve for a strong foam at any given value of x_{D} shows large f_{w} over most of the range of S_{w}, then often an abrupt decrease in f_{w} at the "limiting water saturation" (Khatib et al. 1988; Zhou and Rossen 1995; Rossen et al. 1999; Cheng et al. 2000). For a shear-thinning foam, mobility decreases as the foam bank moves away from the injection well. For foam at fixed fractional flow f_{w}, total relative mobility λ_{rt} is given by

$$\lambda_{rt} = \frac{k_{\mathrm{rw}}(S_{\mathrm{w}})}{\mu_{\mathrm{w}} f_{\mathrm{w}}}. \tag{24}$$

Thus as the bank moves away from the well (x_{D} increases) and foam mobility decreases, the fractional flow curve shifts toward smaller values of S_{w} for a given f_{w}.

4.2 Foam Injection Without Preflush

The MOC solution for this sort of displacement with Newtonian fluids is described by Zhou and Rossen (1995); see Fig. 9a. Typically, surfactant propagation is the limiting factor in foam advance rather than gas, and a gas bank breaks out ahead of the foam bank. The injection condition J is on the foam fractional flow curve at $f_{\mathrm{w}} = f_{\mathrm{w}}^{J}$. The initial condition I is on the fractional flow curve for water and gas without surfactant. Because of the low viscosity of gas without foam, and also the shape of the relative-permeability function for the nonwetting

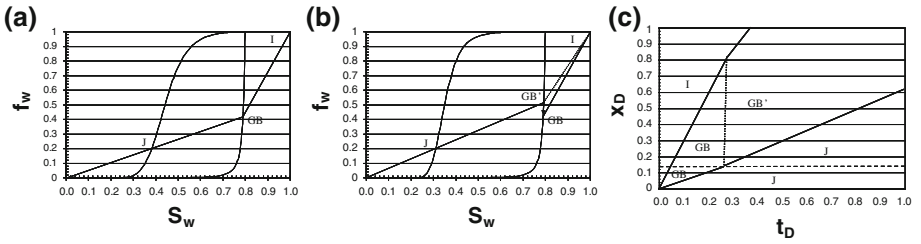

Fig. 9 Schematic of foam fractional flow curve near well (**a**) and further from well (**b**). Also shown in each case is fractional flow curve in the absence of surfactant; this curve does not shift with distance from the well. Also shown is construction of shocks for foam injection without surfactant preflush. In the outer region (**b**), a slightly different gas bank (GB′) is created; it rapidly replaces the gas bank ahead of it (GB) and soon displaces initial condition *I* directly. Velocity of the foam bank increases with distance from well, while mobility within the foam bank decreases. Velocity of the gas bank decreases with distance from well. **c** Schematic time-distance diagram for foam injection without surfactant preflush, for two regions represented in Figs. **a** and **b** (separated by horizontal dashed line in **c**). The gas bank GB′ rapidly replaces initial gas bank GB. Velocity of foam bank increases and velocity of gas bank decreases with distance from well

phase, the fractional flow function $f_w(S_w)$ without foam typically falls from 1.0 to small values for S_w only slightly less than one minus residual gas saturation. A "chemical shock" joins a point on the foam curve to a point on the no-foam curve. The material balances on water and surfactant at this shock correspond to a geometric condition that the points on the two fractional flow curves must lie on a line through a fixed point that depends on the level of surfactant adsorption on the formation (Lake 1989). If adsorption is zero, that point is at ($S_w = 0$, $f_w = 0$). Adsorption moves this fixed point to the left and slows the rate of surfactant propagation; see Zhou and Rossen (1995). For simplicity, we assume here that adsorption is zero.

Consider two schematic regions, one near the well (Fig. 9a) and one further from the well (Fig. 9b). For the inner region, foam is injected at $f_w = f_w^J$. There is a chemical shock defined by a line through (0,0); it passes through J to the foam-free fractional flow curve at *GB*. There is then another shock to I. There are three regions of constant state: J, I, and GB, with uniform f_w in each. Figure 9c (below the horizontal dashed line) shows the $x_D - t_D$ diagram for this displacement.

When the gas bank GB reaches the outer region (Fig. 9c), it displaces I at the same velocity as before; the fractional flow curve without foam is the same in the two regions. When the foam bank reaches the outer region, however, the velocity of the chemical shock is altered because of the shift in the value of S_w corresponding to $f_w = f_w^J$ (Fig. 9b). The gas bank produced downstream of this shock is at GB′, with larger f_w and just slightly larger S_w than in the inner region. Bank GB′ then displaces the gas bank GB ahead of it. Because the fractional flow curve of gas is almost vertical here, the slope of this displacement is very large, and, soon after foam reaches the outer region, GB disappears, to be replaced by GB′. From this point on, gas bank GB′ displaces I.

Consider now a displacement with continuously varying $f_w(S_w, x_D)$. As the foam front advances, the water saturation in the foam bank at each value of x_D is given by the $f_w(S_w)$ curve for the given value of x_D, with $f_w = f_w^J$. The position of the foam bank, x_D^F, at a given time t_D is given by a material balance on surfactant:

$$C_s f_w^J t_D = C_s \int_0^{x_D^F} \left[(S_w)_{f_w = f_w^J} + D \right] dx_D' \tag{25}$$

where C_s the surfactant concentration in the aqueous phase, drops out of this equation, and D is a factor that accounts for surfactant adsorption (specifically, the pore volumes of surfactant solution required to satisfy adsorption in one pore volume of pore space; see Lake (1989) and Zhou and Rossen (1995)), which for simplicity we assume to be zero. Equation 25 can be solved to an arbitrary level of accuracy for the position of the foam bank at any time.

The position of the gas bank is determined by a material balance on gas. Here we assume that at each value of t_D, the newly created bank GB′ quickly overtakes the bank GB upstream; therefore, to a reasonable approximation, the gas bank at any given time t_D is roughly at the gas saturation of the gas bank corresponding to the fractional flow curve for the position x_D^F of the leading edge of the foam bank at that value of t_D. This gives an equation for x_D, the position of the leading edge of the gas bank, as a function of time t_D:

$$\left(1 - f_w^J\right) t_D = \int_0^{x_D^F} (1 - S_w)_{f_w = f_w^J} dx_D{}' + \left(1 - S_w^B\right)\left(x_D - x_D^F\right), \tag{26}$$

where x_D^F is the position of the leading edge of the foam bank at time t_D and S_w^B is the water saturation in the gas bank corresponding to the fractional flow curve at position x_D^F. The first term in Eq. 26 is the gas injected; the second term represents gas in the foam bank, and the third term is an approximation to the gas in the gas bank ahead of foam. This solution is only approximate, because of the assumption that the gas bank is always at the water saturation corresponding to the fractional flow curve that applies at the given value of x_D^F. We expect this approximation to be accurate, however, first, because of the high velocity at which the gas bank responds to the change in the chemical shock, and, second, because the differences in gas saturation between gas banks is not expected to be large (Fig. 9b).

Figure 10 shows the $x_D - t_D$ diagram from a numerical simulation of foam injected into a medium saturated with surfactant-free water. Figure 11 shows $S_w(x_D)$ for $t_D = 0.35$, and, for comparison, the solution from simulation using the same foam parameters and grid resolution as the MOC calculations. The agreement is extremely good on S_w within the foam bank. The finite-difference simulation errs in the position of the foam bank, because of numerical dispersion of surfactant concentration, which affects the imputed position of the chemical shock in the simulations (Rossen et al. 1999; Cheng 2002). The differences in position of the gas bank result from a material balance on gas and the error on position of the foam bank in the simulation. The non-uniformity in S_w in the gas bank in Fig. 11a corresponds to the small wave-like disturbances within the gas bank in Fig. 10. These disturbances result from non-uniform water flux into the gas bank as the foam bank advances one grid block at a time (Cheng 2002). The MOC allows one to plot the variation of S_w and foam strength with position to arbitrary accuracy without simulation; we contend that in this case it is more accurate than simulation on a comparable grid, given the effect of numerical dispersion on the foam front. The MOC solution thus provides a check on the accuracy of simulation under conditions when the assumptions of the MOC apply.

An additional advantage of the MOC is that it is not limited to the level of grid refinement feasible in conventional finite-difference simulation. With the grid spacing of $x_D = 0.01$ in Figs. 10 and 11, the first grid block's outer radius is 50 m (1/100 of the pore volume); within the first grid block superficial velocity changes by a factor of 500, i.e., 90% of the change between the 0.1-m radius wellbore and 500 m. Figure 12a shows the MOC solution corresponding to a region much nearer the wellbore, and Fig. 12b and c compares the resolution of the MOC to the finite-difference solution near the well. Numerical simulation at the level

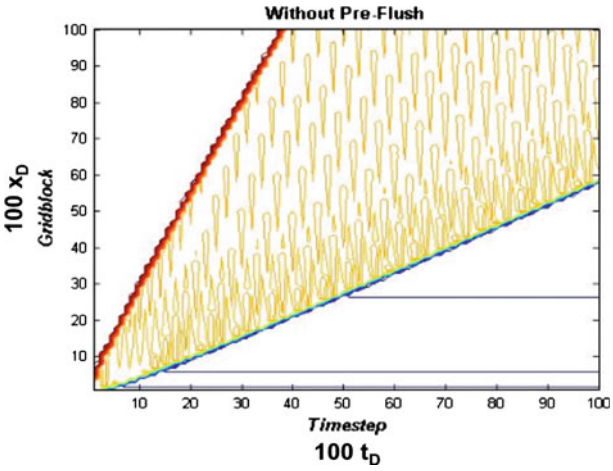

Fig. 10 Time–distance diagram (contour plot of S_w) from finite-difference simulation of foam injection with no preflush. Upper-left region corresponds to initial state I, middle region to gas bank GB, and lower -right region to injected foam J. *Horizontal lines* within region J are not characteristics, but correspond each to a given saturation: from the bottom, 0.33, 0.32, and 0.31, respectively. Within GB, the small wave-like disturbances correspond to water displaced downstream suddenly as each new grid block is invaded by foam. This is an artifact of discretizing position, and the variation of water flux into the gas bank as foam enters each succeeding grid block (Cheng 2002)

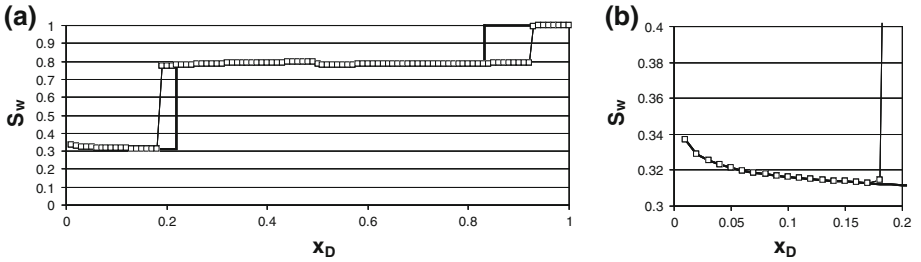

Fig. 11 **a** Water saturation S_w as a function of x_D for $t_D = 0.349$ (MOC solution *solid line*) and $t_D = 0.35$ (simulation *open symbols*). **b** Comparison of S_w within foam bank

of resolution in Fig. 12a would be difficult with a conventional finite-difference approach because of the small volume of grid blocks, but this region is crucial to injectivity.

4.3 Foam Injection Following Surfactant Preflush

In this case, a material balance on gas rather than surfactant limits the advance of the foam front. The position of the leading edge of the foam bank $x_D(t_D)$ is given by

$$\left(1 - f_w^J\right) t_D = \int_0^{x_D} (1 - S_w)_{f_w = f_w^J} \mathrm{d}x_D' \tag{27}$$

where, at each value of x_D, S_w is the value corresponding to the fractional flow curve at x_D with f_w set at f_w^J. There is no gas bank ahead of foam, just initial condition I. Therefore,

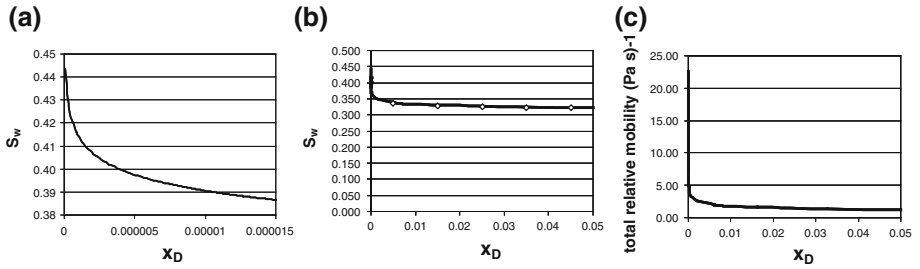

Fig. 12 **a** Water saturation behind shock front, for foam injection for region near wellbore in foam injection. $x_D = 1.5x10^{-5}$ corresponds to about 2 m radius from center of well. **b** Comparison of MOC solution with fine grid (*line*) and finite-difference solution on grid of $\Delta x_D = 0.01$ (*open symbols*) in near-well region. **c** Total relative mobility near well, from MOC solution. Finite-difference solution misses rise in S_w near well, with its implications for mobility (**c**) and injectivity

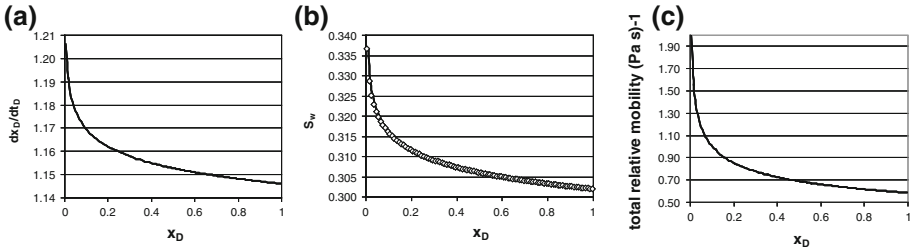

Fig. 13 **a** Velocity of shock front, **b** water saturation **c** total relative mobility behind shock front, for foam injection into preflush. In **b** MOC calculations are compared to finite-difference simulation with the same grid refinement (*open symbols*)

without the approximation involving the gas bank in the preceding section (Eq. 26), the MOC solution for the displacement is exact. Foam mobility as a function of x_D is the same as above. Figure 13 compares the MOC solution with a finite-difference simulation on the same grid.

4.4 Gas Injection into Surfactant Preflush

Creation of foam in a formation by injecting alternating slugs of surfactant solution and gas ("SAG" or "FAWAG" injection) has several advantages over continuous foam injection, including higher injectivity, easer surface operations, and reduced corrosion in piping (Blaker et al. 1999; Shan and Rossen 2004; Kloet et al. 2009). For Newtonian foam, when gas is injected following injection of surfactant solution, the injection condition is at $f_w = 0$, and the initial condition (assuming this is the first slug of gas) is at $S_w = 1$; both points are on the surfactant fractional flow curve; see Fig. 14. As in previous examples, one can allow easily for an immobile oil phase, which we ignore here for simplicity; see Kloet et al. (2009). There is a shock from I to a point of tangency at very low f_w, and a rarefaction wave behind it.

Each characteristic in the rarefaction wave moves downstream with unchanging f_w. There are few data on the fractional flow curve in this low range of f_w (Kibodeaux and Rossen 1997; Wassmuth et al. 2001; Xu and Rossen 2004), much less how this curve shifts for non-Newtonian foam. Because mobility is lower downstream, and the fractional flow curve shifts toward smaller values of S_w as one moves downstream, one expects that the curve becomes steeper at a given value of f_w, as illustrated in Fig. 15. This implies that the velocities of

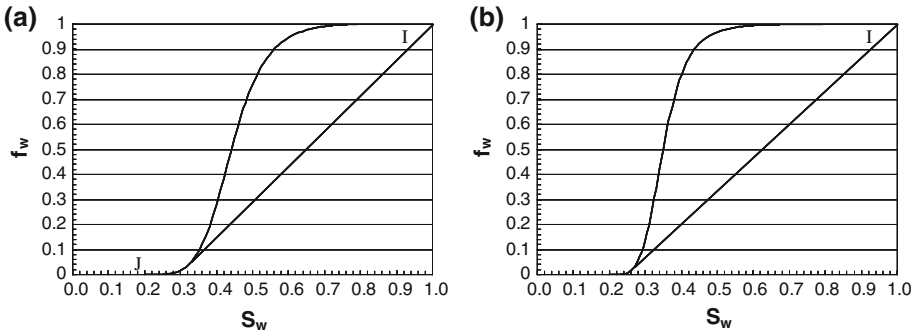

Fig. 14 Schematic of foam fractional flow curve near well (**a**) and further from well (**b**), where foam mobility is lower. Also shown in each case is construction of shocks for gas injection in a SAG process assuming same fractional flow curve applies throughout the medium. One expects velocity of shock to increase, and range of water saturations behind shock to decrease, as the front moves further from the well

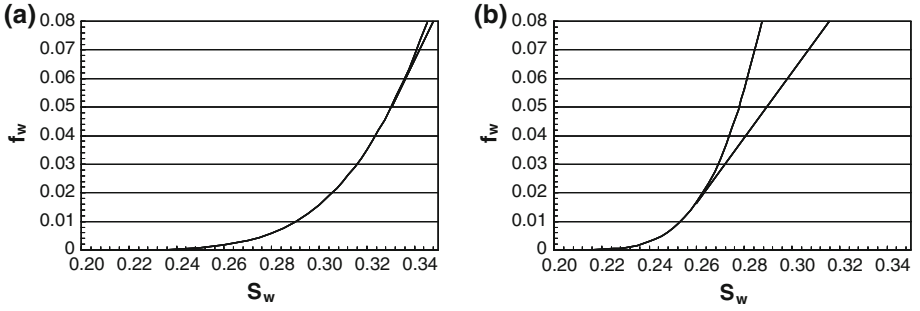

Fig. 15 Expanded view of Fig. 14 near point of shock tangency. In reality, the shock is not defined by any simple graphical construction, except at the injection face; the velocity of the shock changes as the result of collisions between faster-moving characteristics with the shock and the slowing of the shock itself. This construction illustrates that the velocity of characteristics corresponding to any given value of f_w behind the shock increases with distance from the well

the individual characteristics increase downstream. At the same time, the point of tangency moves to lower S_w, which implies a decrease in the velocity of the shock. Both factors suggest that characteristics just behind the shock at small x_D collide with the shock as they move downstream. The solution is complex. Except at the inlet face, the shock is not determined as a point of tangency to the fractional flow curve for that position, but is the result of colliding characteristics from behind as well as the condition ahead. Figure 16 illustrates the process as resolved by finite-difference simulation.

As the displacement proceeds, however, these collisions occur further and further downstream, and the region near the well contains curving characteristics that can be computed without accounting for the shock. Figure 17a compares water saturation behind the shock at dimensionless position $x_D = 0.20$ computed by finite-difference simulation and the MOC on the same grid; the agreement is excellent. Figure 17b shows how water saturation varies as a function of time for a position very near the well in radial flow conditions near the well control injectivity of the gas, an important consideration for overcoming gravity override (Shan and Rossen 2004; Kloet et al. 2009; Jamshidnezhad et al. 2008). The MOC allows computation of injectivity in a dynamic SAG process with non-Newtonian fluids without the need for, and to greater accuracy than, simulation.

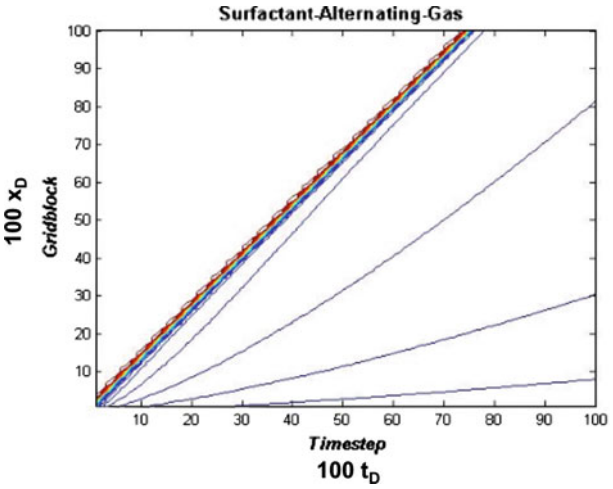

Fig. 16 Time-distance diagram (contour plot of S_w) from finite-difference simulation of gas injection in a SAG process. Upper-left region corresponds to initial state I, and lower-right region to rarefaction wave upstream of shock; condition J is the horizontal axis. Curves within region J are not characteristics (which have constant f_w rather than constant S_w) but correspond each to a given saturation: 0.23, 0.24, 0.25, and 0.26 starting from the horizontal axis

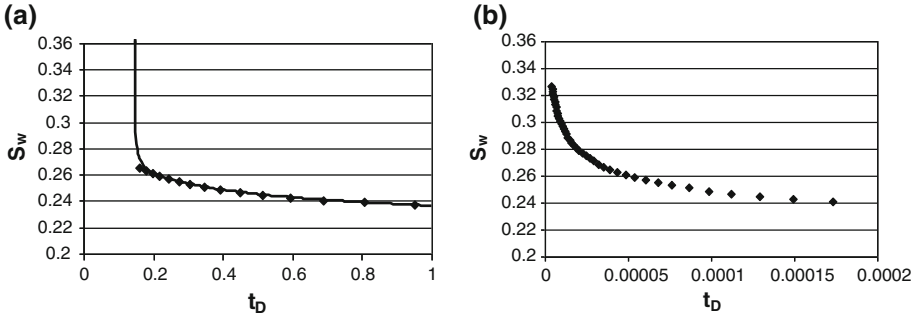

Fig. 17 **a** Water saturation at position $x_D = 0.20$ as a function of dimensionless time t_D, after passage of the shock, from finite-difference simulation (*continuous curve*) and MOC solution behind the shock (*points*). Computing the position of the shock using the MOC would be complex in this case. **b** Water saturation at position $x_D = 3.2x10^{-6}$ (radial position 90 cm) as a function of t_D, after passage of the shock, from MOC solution behind the shock. The shock would pass this position at time $t_D < 3.2x10^{-6}$, before any of the points shown

5 Conclusions

- A methodology is described for solving dynamic 1D fractional flow problems involving non-Newtonian fluids in non-rectilinear flow.
- For polymers that show Newtonian behavior at low and high shear rates and behave as a power-law fluid in between, a semi-analytical solution using the MOC is developed that leads to generation of shocks and characteristics colliding with shocks. The analytical solution matches well with the finite difference simulation for the particular parameter values considered. Such solutions offer more accurate resolution of saturations and mobility near the well, and therefore better estimates of injectivity in polymer EOR.

- For foam injection into a medium saturated with water and no surfactant, one can solve exactly for the position and mobility of the foam bank, and to good accuracy for the position of the gas bank ahead of the foam. In the example shown, the position of the foam and gas banks are resolved more accurately by the MOC than by finite-difference simulation on the same grid, because of the adverse effect of numerical dispersion on surfactant concentration in the simulations. Mobility of the foam bank changes substantially with radial position, especially very near the well. This variation would be difficult to resolve by finite-difference simulation with practical grid-block sizes.
- Solution by MOC is exact for the case of foam injection following a surfactant preflush.
- During gas injection in a SAG process, characteristics collide with the shock during the displacement and the solution for the shock is complex. However, one can conclude from the fractional flow curves that the shock slows down and shifts to lower water saturation and lower mobility as it moves further from the well. The mobility near the well can be determined by the MOC without solving for the shock velocity. These predictions agree well with computer simulations of such a process.

Acknowledgments Marco Kloet provided software we used in the MOC analysis of foam examples. Yang Dong wrote the software used in finite-difference simulations for foam.

Appendix A: Polymer Model

Derivation of the Characteristic Equations

We assume that the viscosity of aqueous polymer solution depends on its interstitial velocity. For a power-law polymer fluid

$$\mu_{\mathrm{w}} = \mu_{\mathrm{w}}^{\mathrm{o}} \left(\frac{v_{\mathrm{w}}}{v_{\mathrm{w}}^{\mathrm{o}}} \right)^{n-1}, \tag{A1}$$

where $\mu_{\mathrm{w}}^{\mathrm{o}}$ is the reference viscosity of the aqueous phase, $v_{\mathrm{w}}^{\mathrm{o}}$ is the reference velocity of the aqueous phase, n is the fluid power-law exponent, and

$$v_{\mathrm{w}} = \frac{u f_{\mathrm{w}}}{S_{\mathrm{w}} \phi}; \mu_{\mathrm{w}} = \mu_{\mathrm{w}}^{\mathrm{o}} \left(\frac{u f_{\mathrm{w}}}{v_{\mathrm{w}}^{\mathrm{o}} S_{\mathrm{w}} \phi} \right)^{n-1}, \tag{A2}$$

where u is the total superficial velocity. We group the parameters as

$$\frac{u}{v_{\mathrm{w}}^{\mathrm{o}} \phi} = \frac{Q}{2\pi r h v_{\mathrm{w}}^{\mathrm{o}} \phi} = \frac{Q}{2\pi r_{\mathrm{e}} \phi h v_{\mathrm{w}}^{\mathrm{o}} \sqrt{x_{\mathrm{D}}}} \equiv \frac{Q_{\mathrm{D}}}{\sqrt{x_{\mathrm{D}}}}; \; Q_{\mathrm{D}} \equiv \frac{Q}{2\pi r_{\mathrm{e}} h v_{\mathrm{w}}^{\mathrm{o}}}. \tag{A3}$$

The reference velocity $v_{\mathrm{w}}^{\mathrm{o}}$ is constant so that increasing injection rate gives larger Q_{D}. Substitution of the non-Newtonian fluid-viscosity equation in terms of Q_{D} into the definition of f_{w} yields

$$f_{\mathrm{w}} = \frac{1}{1 + \frac{k_{\mathrm{o}} \mu_{\mathrm{w}}^{\mathrm{o}}}{k_{\mathrm{w}} \mu_{\mathrm{o}}} \left(\frac{Q_{\mathrm{D}} f_{\mathrm{w}}}{\sqrt{x_{\mathrm{D}}} S_{\mathrm{w}}} \right)^{n-1}} \tag{A4}$$

Here k_{o} and k_{w} are the relative permeability functions for oleic and aqueous phases, respectively, and μ_{o} is the viscosity of the oleic phase. For integer values of n, Eq. A4 can be rearranged into a polynomial equation for f_{w}, but for most $n < 1$ (shear-thinning fluids)

it must be solved by iteration. This is the case where the fractional flow curve (f_w vs. S_w) changes with the distance from the injection well (x_D).

We assume a Corey type relative permeability correlation with n_w and n_o as the water and oil exponents, respectively, and S (normalized water saturation) given by following relation between S_w (water saturation), S_{wr} (residual water saturation) and S_{or} (residual oil saturation):

$$k_o = k_o^{end}(1-S)^{n_o};\ k_w = k_w^{end}(S)^{n_w};\ M_{ref}^o = \frac{k_w^{end}}{k_o^{end}};\ S = \frac{S_w - S_{wr}}{1 - S_{or} - S_{wr}} \tag{A5}$$

We define function H and have the following relations:

$$H(S_w, x_D) \equiv \frac{k_{ro}\mu_w^o}{k_{rw}\mu_o}\left(\frac{Q_D}{\sqrt{x_D}S_w}\right)^{n-1} = \frac{(1-S)^{n_o}}{M_{ref}^o S^{n_w}}\left(\frac{Q_D}{\sqrt{x_D}S_w}\right)^{n-1} \tag{A6}$$

$$\left(\frac{\partial H}{\partial x_D}\right)_{s_w} = \left(\frac{1-n}{2}\right)\left(\frac{(Q_D)^{n-1}}{M_{ref}^o}\right)\left(\frac{(1-S)^{n_o}}{S^{n_w}S_w^{n-1}}\right)\left(\frac{1}{x_D}\right)^{n+1} \tag{A7}$$

$$\left(\frac{\partial H}{\partial S_w}\right)_{x_D} = \left(\frac{(Q_D)^{n-1}}{M_{ref}^o}\right)\left(\frac{(1-S)^{n_o}}{S^{n_w}S_w^{n-1}}\right)\left(\frac{-n_0}{1-S} + \frac{(-n_w)}{S} + \frac{(1-n)}{S_w}\right)\left(\frac{1}{\sqrt{x_D}}\right)^{n-1} \tag{A8}$$

The general form of the fractional flow f_w (Eq. A4) can be now be written as:

$$f_w = \frac{1}{1 + H(f_w)^{n-1}}. \tag{A9}$$

We develop the equations further for a particular case when $n = 0.5$. Equation A4 reduces to a quadratic equation for $\sqrt{f_w}$ for a given saturation S_w:

$$f_w = \left(\frac{-H + \sqrt{H^2+4}}{2}\right)^2 \tag{A10}$$

For this case, H is given by,

$$H(S_w, x_D, n = 0.5) = \frac{(1-S)^{n_o}}{M_{ref}^o S^{n_w}}\left(\frac{Q_D}{\sqrt{x_D}S_w}\right)^{-0.5} \tag{A11}$$

We can differentiate to get relations:

$$\left(\frac{\partial f_w}{\partial S_w}\right)_{x_D} = H\left(H - \frac{H^2+2}{\sqrt{H^2+4}}\right)\left(\frac{-n_0}{(1-S)(1-S_{rw}-S_{ro})} + \frac{(-n_w)}{S(1-S_{rw}-S_{ro})} + \frac{(1-n)}{S_w}\right) \tag{A12}$$

$$\left(\frac{\partial f_w}{\partial x_D}\right)_{S_w} = \left(H - \frac{H^2+2}{\sqrt{H^2+4}}\right)\left(\frac{H}{4x_D}\right) \tag{A13}$$

Showing f_w Is a Constant

We can represent H as

$$H(S_w, x_D) = \left(\frac{(Q_D)^{n-1}}{M_{ref}^o}\right) m(Sw)n(x_D), \tag{A14}$$

where $m(S_w)$ and $n(x_D)$ and are functions such that

$$m(Sw) = \frac{(1-S)^{n_o}}{S^{n_w} S_w^{n-1}}; n(x_D) = \left(\frac{1}{\sqrt{x_D}}\right)^{n-1} \tag{A15}$$

We have the following relations:

$$\left(\frac{\partial H}{\partial x_D}\right)_{s_w} = \left(\frac{(Q_D)^{n-1}}{M_{ref}^o}\right) m(Sw) n'(x_D) \tag{A16}$$

$$\left(\frac{\partial H}{\partial S_w}\right)_{x_D} = \left(\frac{(Q_D)^{n-1}}{M_{ref}^o}\right) n(x_D) m'(Sw) \tag{A17}$$

We can combine the two characteristic equations (Eqs. 12 and 13) to get,

$$\frac{dS_w}{dx_D} = \frac{-\left(\frac{\partial H}{\partial x_D}\right)_{s_w}}{\left(\frac{\partial H}{\partial S_w}\right)_{x_D}} = \frac{-\left(\frac{(Q_D)^{n-1}}{M_{ref}^o}\right) m(Sw) n'(x_D)}{\left(\frac{(Q_D)^{n-1}}{M_{ref}^o}\right) n(x_D) m'(Sw)} \tag{A18}$$

We can simplify and integrate the above differential equation as,

$$\int \frac{m'(Sw)\mathrm{d}S_w}{m(Sw)} = \int \frac{-n'(x_D)\mathrm{d}x_D}{n(x_D)} + k. \tag{A19}$$

This gives

$$m(Sw) n(x_D) = c_1, \tag{A20}$$

where c_1 is a constant. Substitution of the values of functions ($m(S_w)$ and $n(x_D)$) and multiplying by the constant $\left(\frac{(Q_D)^{n-1}}{M_{ref}^o}\right)$gives,

$$\left(\frac{(Q_D)^{n-1}}{M_{ref}^o}\right) \frac{(1-S)^{n_o}}{S^{n_w} S_w^{n-1}} \left(\frac{1}{\sqrt{x_D}}\right)^{n-1} = H = c_2, \tag{A21}$$

where c_2 is another constant. Thus along a characteristic the function H is a constant. We can also infer from Eq. A10 that f_w is constant along the characteristic when H is constant.

Appendix B: Foam Model Parameters

We assume fluid and formation properties as specified in Table B1. We assume that where foam exists it reduces gas mobility by a factor R. For simplicity, we represent this effect as a reduction in gas relative permeability and leave the gas viscosity unaffected by foam (Rossen et al. 1999). For shear-thinning foam, we assume R is a power-law function of total superficial velocity, and therefore a power-law function of x_D:

$$k_{rg}^f = \frac{k_{rg}^o(S_w)}{R(x_D)} = \frac{k_{rg}^o(S_w)}{R_o x_D^{(1-n)/2}}, \tag{B1}$$

where k_{rg}^f and k_{rg}^o are gas relative permeability in the presence or absence of foam, and R_o is the gas mobility reduction that applies at the outer radius, i.e., $x_D = 1$.

We solve the fractional flow Eqs. 25–27 (with $D = 0$, corresponding to no adsorption), along with the velocities of the characteristics for SAG injection behind the shock front, on

Table B1 Parameters used in foam examples

Cylindrical reservoir: r_w, r_e	0.1 m, 500 m
Number of grid blocks N	100 (linear in $x_D \sim \sqrt{r}$)
Porosity	0.25
Water viscosity	0.001 Pa s
Gas viscosity	0.00002 Pa s
Water relative permeability function	$0.20\,[(S_w - 0.2)/0.6]^{4.2}$
Gas relative permeability function w/o foam	$0.657[(0.8 - S_w)/0.6]^{1.3}$
Gas mobility reduction factor Ro (Eq. A1)	55,000

a grid with intervals of 0.01 in x_D, except where noted in the text. This corresponds to the same resolution used in the numerical simulations described next.

The numerical simulations use a simple forward-difference finite-difference scheme, and assume a 1D incompressible displacement. That is, for each time step l we solve

$$S_{wk}^{l+1} = S_{wk}^{l} + \frac{\Delta t_D}{\Delta x_D}\left(f_{wk-1}^{l} - f_{wk}^{l}\right) \tag{B2}$$

for grid blocks $k = 1, \ldots, N$, where f_w is a function of both S_{wk} and k. After this step the concentration of surfactant at all locations is updated according to

$$c_{sk}^{n+1} = \left[c_{sk}^{n} S_{wk}^{n} + \frac{\Delta t_D}{\Delta x_D}\left(c_{sk-1}^{n} f_{wk-1}^{n} - c_{sk}^{n} f_{wk}^{n}\right)\right] / S_{wk}^{n+1} \tag{B3}$$

where c_{sk}^{n} is the concentration of surfactant, assumed soluble only in the water phase. In the absence of dispersion, surfactant concentration in the aqueous phase takes only two values, zero and the injected concentration (or initial concentration in a case with a preflush) C_s^o. In numerical calculations, dispersion spreads the front in surfactant concentration over many grid blocks. To minimize the effect of dispersion in simulations (Rossen et al. 1999; Cheng 2002), we make foam creation a step function of surfactant concentration:

For $C_s \le C_s^o/2$,

$$k_{rg} = k_{rg}^{o}(S_w) \tag{B4}$$

For $C_s > C_s^o/2$,

$$k_{rg} = \frac{k_{rg}^{o}(S_w)}{R_o\left(\left(k - \frac{1}{2}\right)/N\right)^{(1-n)/2}} \tag{B5}$$

where k is the given grid-block number and N the total number of grid blocks. For foam injection with surfactant preflush, $C_s = C_s^o$ everywhere and only Eq. B1 applies. For foam injection, the injected water has $C_s = C_s^o$.

In reality, "strong" foam at steady state can exist in two regimes, depending on foam quality and capillary pressure (Osterloh and Jante 1992; Alvarez et al. 2001). The two regimes have different, potentially non-Newtonian characteristics. Also, gas mobility abruptly increases in the vicinity of the "limiting water saturation" (Khatib et al. 1988; Zhou and Rossen 1995). The relatively small value of power-law exponent n here (0.5; see Table B1) reflects behavior in the "low-quality regime," i.e., far from dry conditions of foam collapse. We have assumed a particularly simple foam model here to illustrate the effects of shear-thinning rheology without the other complications of foam behavior. The methods described here could be easily applied to other cases of non-Newtonian behavior. See Table B1.

References

AlSofi, A.M., Blunt, M.J.: Streamline-based simulation of non-Newtonian polymer flooding. SPE J. **15**, 901–911 (2010)

Alvarez, J.M., Rivas, H., Rossen, W.R.: A unified model for steady-state foam behavior at high and low foam qualities. SPE J. **6**, 325–333 (2001)

Bedrikovetsky, P.: Mathematical Theory of Oil and Gas Recovery. Kluwer Academic Publishing, The Netherlands (1993)

Bird, R.B., Stewart, W.E., Lightfoot, E.N.: Transport Phenomena, 2nd ed. Wiley, New York (2002)

Blaker, T., Celius, H.K., Lie, T., Martinsen, H.A., Rasmussen, L., Vassenden, F.: Foam for gas mobility control in the snorre field: the FAWAG project. Paper SPE 56478, Presented at the 1999 SPE Annual Technical Conference and Exhibition, Houston, TX, 3–6 October 1999

Cheng, L.: Simulation studies of foam-acid diversion. PhD Dissertation, The University of Texas at Austin (2002)

Cheng, L., Reme, A.B., Shan, D., Coombe, D.A., Rossen, W.R.: Simulating foam processes at high and low foam qualities. Paper SPE 59287, Presented at the 2000 SPE/DOE Improved Oil Recovery Symposium, Tulsa, OK, 3–5 April 2000

Jamshidnezhad, M., Chen, C., Kool, P., Rossen, W. R.: Well stimulation and gravity segregation in gas improved oil recovery. Paper SPE 112375, Presented at the 2008 SPE International Symposium and Exhibition on Formation Damage Control held in Lafayette, Louisiana, USA, 13–15 February 2008; accepted for publication in SPE Reserv. Eval. Eng

Khatib, Z.I., Hirasaki, D.J., Falls, A.H.: Effects of capillary pressure on coalescence and phase mobilities in foams flowing through porous media. SPERE **3**, 919–926 (1988)

Kibodeaux, K.R., Rossen, W.R.: Coreflood study of surfactant-alternating-gas foam processes. Paper SPE 38318, Presented at the 1997 SPE Western Regional Meeting, Long Beach, CA, 25–27 June 1997

Kloet, M.B., Renkema, W.J., Rossen, W.R.: Optimal design criteria for SAG foam processes in heterogeneous reservoirs. Paper SPE 121581, Presented at the 2009 SPE EUROPEC/EAGE Annual Conference and Exhibition, Amsterdam, The Netherlands, 8–11 June 2009

Kovscek, A.R. Radke, C.J.: Fundamentals of foam transport in porous media. In: Schramm, L.L. (ed.), Foams: Fundamentals and Applications in the Petroleum Industry. ACS Advances in Chemistry Series No. 242, Washington, DC (1994)

Lake, L.: Enhanced Oil Recovery. Prentice Hall, Englewood Cliffs, NJ (1989)

Osterloh, W.T., Jante, M.J.: Effects of gas and liquid velocity on steady-state foam flow at high temperature. SPE 24179, SPE/DOE on EOR, Tulsa, OK, 22–24 April 1992

Pope, G.A.: The application of fractional flow theory to enhanced oil recovery. SPE J. **10**, 191–205 (1980)

Rhee, H., Aris, R., Amundson, N.: First-Order Partial Differential Equations. Prentice Hall, Englewood Cliffs, NJ (1986)

Rong, J.G.: Experimental evaluation of foam in environmental remediation. PhD Dissertation, The University of Texas at Austin (2002)

Rossen, W.R.: Foams in enhanced oil recovery. In: Prud'homme, R.K., Khan, S. (eds.) Foams: Theory, Measurement, and Applications, Marcel Dekker, New York (1996)

Rossen, W.R., Zeilinger, S.C., Shi, J.-X., Lim, M.T.: Simplified mechanistic simulation of foam processes in porous media. SPE J. **4**, 279–287 (1999)

Shan, D., Rossen, W.R.: Optimal injection strategies for foam IOR. SPE J. **9**, 132–150 (2004)

Subramanian, S., Johns, R.T., Dindoruk, B.: Effect of fractional flow heterogeneity on compositional and immiscible displacements. Proceedings of 9th European Symposium on Improved Oil Recovery, The Hague, The Netherlands, Paper no. 060, October 20–22 (1997)

Subramanian, S.K., Johns, R.T., Dindoruk, B.: Solution and upscaling of compositional and immiscible displacements in composite media. Petrol. Geosci. **5**, 287 (1999)

Venkatraman, A., Johns, R.T., Rossen, W.R.: Fractional flow theory for non-Newtonian Polymer Flooding. Proceedings of 16th European Symposium on Improved Oil Recovery, Cambridge, UK, 12–14 April 2011

Walsh, M.P., Lake, L.W.: Applying fractional flow theory to solvent flooding and chase fluid. J. Petrol. Sci. Eng. **2**, 281–303 (1989)

Wassmuth, F.R., Green, K.A., Randall, L.: Details of in-situ foam propagation exposed with magnetic resonance imaging. SPEREE, 135–145, April 2001

Wu, Y.S., Pruess, K., Witherspoon, P.A.: Displacement of a Newtonian fluid by a non-Newtonian fluid in a porous medium. Transp. Porous Media **6**, 115–142 (1991)

Wu, Y.S., Pruess, K., Witherspoon, P.A.: Flow and displacement of bingham non-newtonian fluids in porous media. SPERE **7**, 369–376 (1992)

Wu, Y.S., Pruess, K., Chen, X.Z.: Buckley–Leverett flow in composite porous media. SPE Adv. Technol. **1**(2), 36 (1995)

Xu, Q., Rossen, W.R.: Experimental study of gas injection in surfactant-alternating-gas foam process. SPE Reserv. Eval. Eng. **7**, 438–448 (2004)

Yi, X.: Model for displacement of Herschel–Bulkley non-Newtonian fluid by newtonian fluids in porous media and its application in fracturing-fluid cleanup. Paper SPE 86491, Presented at the Formation Damage Symposium, Lafayette, LA, 18–20 February 2004

Zhou, Z.H., Rossen, W.R.: Applying fractional-flow theory to foam processes at the "limiting capillary pressure". SPE Adv. Technol. **3**(1), 154–162 (1995)